Winding Factors and Harmonics of Coreless Axial Flux PM Machines

Matin Vatani
SPARK Lab, Pigman Eng. College
University of Kentucky
Lexington, KY, USA
matin.vatani@uky.edu

John F. Eastham
Dept. of Electronic & Electrical Eng.
University of Bath
Claverton Down, Bath, UK
jfeastham@aol.com

Xiaoze Pei
Dept. of Electronic & Electrical Eng.
University of Bath
Claverton Down, Bath, UK
X.Pei@bath.ac.uk

Dan M. Ionel
SPARK Lab, Pigman Eng. College
University of Kentucky
Lexington, KY, USA
dan.ionel@ieee.org

***Abstract*—This paper provides a comprehensive analysis of the winding factor and winding harmonic distribution in coreless stator axial flux permanent magnet (AFPM) machines. The topology of this type of machine and its similarities to conventional cored AFPM machines are discussed. Popular pole/coil number combinations in coreless stator AFPM machines are identified and analyzed in detail. It is demonstrated that the winding factor in these machines varies with radius and can be expressed as the product of the conductor distribution factor, pitch factor, and coil group factor. The formulas for each factor are derived and presented in multiple forms based on different parameters. The winding factors for the considered pole/coil combinations are calculated under different conditions, and their corresponding harmonic distributions are compared. The results indicate that certain pole/coil combinations yield higher winding factors, improving torque capability.**

***Index Terms*—Axial flux permanent magnet machine, coreless stator, winding factor, pole/coil ratio, winding harmonic analysis.**

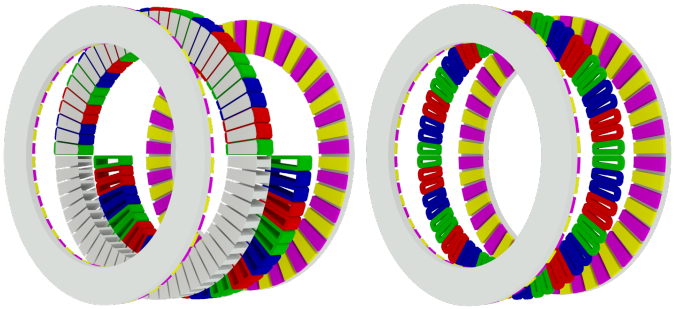

(a) (b)

Fig. 1. Axial flux PM machines with a 10/12 pole-to-coil ratio, illustrating (a) a yokeless and segmented armature (YASA) topology with ferromagnetic teeth and (b) a coreless stator configuration, which does not employ any ferromagnetic material in the stator.

I. Introduction

According to a forecast by Industry ARC, the axial flux machine market is projected to grow at an average annual rate of 11.90% from 2024 to 2030 [1]. Axial flux PM machines offer several advantages over conventional radial flux machines, particularly a higher power-to-mass ratio in a more compact form factor [2]. These machines are well suited for applications requiring a short axial length relative to the outer diameter, such as in-wheel drives, and those demanding high inertia, such as flywheels [3, 4].

These machines can accommodate a high number of poles, which has been shown to reduce overall mass as the pole count increases [5], making them well-suited for low-speed applications such as fans and electric machinery [6]. Their structure also enables more efficient direct cooling compared to radial flux machines, as demonstrated in [7, 8], allowing their use in high-performance applications such as electric vehicles. Furthermore, their axially compact design facilitates the integration of multiple AFPM machines on the same shaft, enhancing both power output and reliability while maintaining the same outer diameter [9, 10]. This makes them particularly suitable for aircraft and direct-drive generators.

A variation of AFPM machines is the coreless stator design, which generates torque based on the Lorentz force theorem through the interaction between rotor flux density and current-carrying conductors [11, 12]. An example of a coreless stator AFPM machine is presented and compared with a conventional yokeless and segmented armature (YASA) AFPM machine in Fig. 1. In YASA topology, concentrated coils are wound around ferromagnetic teeth. Eliminating both these teeth and the stator core can result in lighter machines with higher efficiency since the core and tooth-related losses are removed [13–15].

Given the advantages of coreless AFPM machines, they have been explored for various applications using different topologies and materials. For example, the absence of a stator core allows for the implementation of printed circuit board (PCB) stators [16–18]. Using PCB stators offers significant benefits, including cost-effective and fully automated manufacturing [19]. This type of winding has been adopted

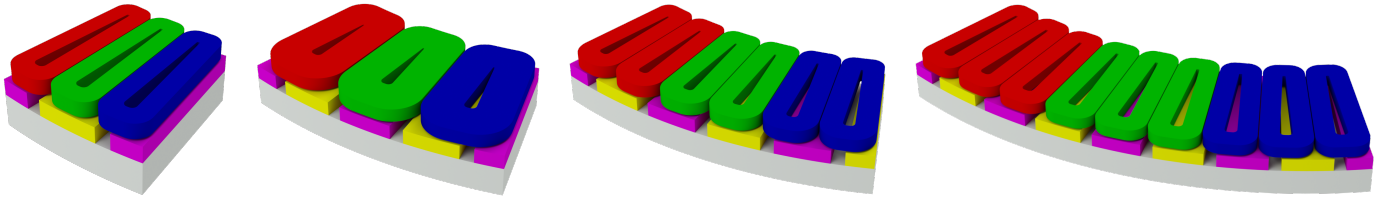

(a) (b) (c) (d)

Fig. 2. Coreless stator AFPM machines, which may employ ferromagnetic material only in the rotor, illustrating one circumferential symmetry for pole-to-coil ratios: (a) 2/3, (b) 3/4, (c) 10/12 (and 14/12), and (d) 8/9 (and 10/9).

Table I
BASE POLE-COIL COMBINATIONS FOR CONCENTRATED THREE-PHASE WINDING CORELESS STATOR AFPM MACHINES. THE SYMMETRY COEFFICIENT SPECIFIES THE CIRCUMFERENTIAL SECTION REQUIRED FOR ELECTROMAGNETIC MODELING.

Pole Num. (P) [-]	Coil Num. (N_c) [-]	Sym. Coeff. [mech. deg.]	Phase Diff. [elec. deg]	Phase Grp. [-]
2	3	$\frac{4\pi}{P}$	120	1
4	3	$\frac{8\pi}{P}$	240	1
10	12	$\frac{10\pi}{P}$	120	2
14	12	$\frac{14\pi}{P}$	240	2
8	9	$\frac{16\pi}{P}$	120	3
10	9	$\frac{20\pi}{P}$	240	3

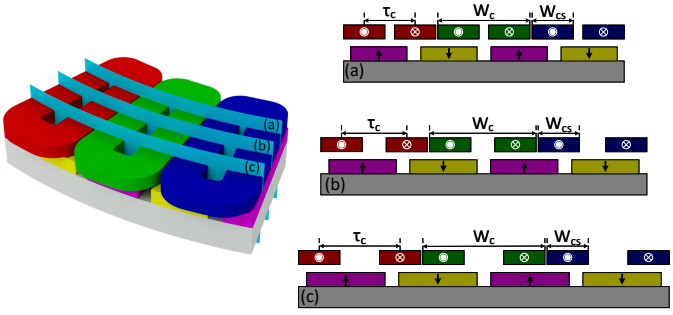

(a) (b)

Fig. 3. Illustration of the curvature effect, i.e., radii dependency of rotor and stator geometries in AFPM machines, demonstrated by three cylindrical cuts and their unrolled representations as equivalent linear machines.

in numerous commercial and research projects for coreless stator AFPM machines of various sizes and ratings. Examples include the application in fan and pump systems by Infinitum Electric, Inc. [20] and E-Circuit Motors, Inc. [21], as well as large direct-drive generators by Boulder Wind Turbine [22].

The higher power-to-mass ratio of coreless AFPM machines compared to their cored counterparts makes them strong candidates for aircraft propulsion systems [23]. For instance, LaunchPoint Electric Propulsion Solutions, Inc. manufactures coreless AFPM machines with Halbach PM array rotors for aerospace propulsion applications [24–26]. Additionally, their lightweight nature makes them well-suited for direct-drive wind turbine generators. Their reduced mass, absence of normal forces between the stator and rotor, and lower normal forces between rotors minimize the weight of mechanical components and simplify generator assembly [27, 28]. Several examples of such implementations can be found in [29–31].

The growing interest in coreless AFPM machines necessitates a thorough analysis of their characteristics. While the rotor field analysis has been extensively detailed in [11], research on stator winding factors and harmonic analysis remains limited. Several studies have focused on calculating the winding factor for coreless stator linear machines [32–34]; however, these methods do not account for the curvature effects present in coreless stator AFPM machines. This paper introduces a comprehensive method for analyzing the winding factor and harmonic distribution in coreless stator AFPM machines across various pole/coil combinations.

II. POLE-TO-COIL RATIOS IN CORELESS STATOR AFPM MACHINES

Coreless stator AFPM machines can utilize pole-coil combinations similar to those of slotted machines. Various pole/coil configurations were comprehensively analyzed in [35]. The most popular pole/coil combinations for coreless stator AFPM machines are summarized in Table I, including a three-coil design compatible with two or four poles, a nine-coil design compatible with eight or ten poles, and a twelve-coil design compatible with ten or fourteen poles.

Different Pole/coil combinations in example designs are shown in Fig. 2. Since the 14/12 ratio resembles 10/12, and 10/9 is similar to 8/9, they are omitted to avoid redundancy. Table I provides detailed information on circumferential symmetry boundaries, phase differences, and the number of coil groups per phase. The symmetry coefficient specifies the circumferential section required for electromagnetic modeling, the phase difference represents the electrical angle between phases, and the phase group defines the number of adjacent coils within each phase.

III. HARMONIC ANALYSIS OF WINDINGS

To determine the winding factor for a coreless winding phase, the process by first calculating the distribution factor for an individual coil and then summing the contributions of all coils within the phase. The coil distribution factor is obtained by multiplying the conductor distribution and the coil pitch (or chording) factors. Finally, for pole/coil combinations where the

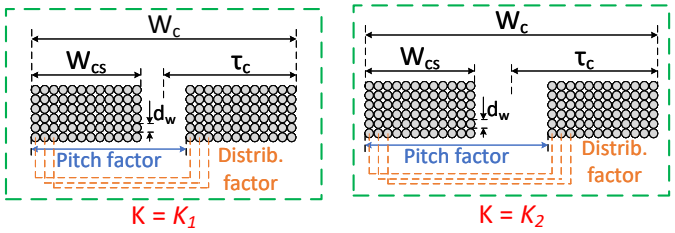

Fig. 4. Radial cut-out of a coil at two radii: (a) smaller radius and (b) larger radius, highlighting the impact of radius on the conductor distribution and pitch factors.

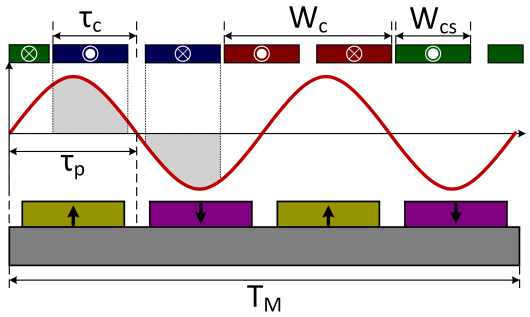

Fig. 5. Two-dimensional visualization of the conductor distribution and pitch factors in four poles and three coils configuration.

coil group number exceeds one, the coil group factor must be considered.

This section develops generalized equations for calculating these factors in coreless stator AFPM machines, considering the radial variation of coil geometry. The derived formulas enable the computation of the winding factor at any arbitrary radius, and the overall winding factor may be determined as the average of the winding factors across different radii.

A. Conductor Distribution Factor

Single general machine winding consisting of a group of coils connected in series is equivalent to a series connection of ideal sinusoidally distributed winding harmonically related in space distribution. The conductor distribution can then be expressed as a Fourier expansion with a zero average term:

$$N = \sum_{\nu=1}^{\infty} N_\nu \cos\left(\nu\theta + \varphi_\nu\right), \tag{1}$$

where N_ν is the amplitude of the νth harmonic and φ_ν is the phase angle.

Since the conductor distribution cannot be expressed in angular coordinates for coreless stator axial flux machines due to the uniform width of coil sides across all radii, the Fourier expansion of the conductor distribution can be found

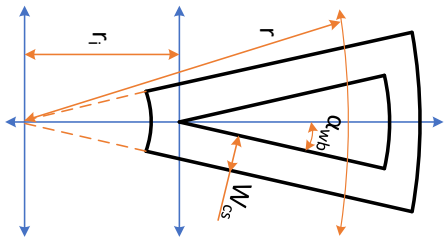

Fig. 6. Top view of a coil showing geometric parameters.

as a radius-dependent equation as:

$$\begin{aligned} N &= \sum_{\nu=1}^{\infty} N_\nu \cos\left(\nu\frac{x}{r} + \frac{x_\nu}{r}\right) \\ &= \frac{N_t}{2}\sum_{\nu=1}^{\infty} e^{j\left(\frac{\nu x}{r}+\frac{x_\nu}{r}\right)} + e^{-j\left(\frac{\nu x}{r}+\frac{x_\nu}{r}\right)} \\ &= \frac{\overline{N_t}}{2}\sum_{\nu=1}^{\infty} e^{j\left(\frac{\nu x}{r}\right)} + e^{-j\left(\frac{\nu x}{r}\right)} \end{aligned} \tag{2}$$

$$\overline{N_t} = N_t e^{j\left(\frac{\nu x_\nu}{r}\right)} = \frac{1}{\pi}\int_0^{2\pi} F(x) e^{-j\left(\frac{\nu x}{r}\right)} dx, \tag{3}$$

where x and r are the position and radius at which the conductor distribution is evaluated.

Consider a cut at an arbitrary radius of a coreless stator AFPM machine, corresponding to the smallest required circumferential segment described in Table I, and unroll it to form a linear machine. If a coil side is located at W_s containing N_s conductors and has a width of W_{cs}, as illustrated in Fig. 4, the conductor distribution generated by the coil side over the total width of one periodicity T_M of the considered section is:

$$\begin{aligned} \overline{N_t} &= \frac{2}{T_M}\int_{\frac{2\pi}{T_M}\left(W_s-\frac{W_{cs}}{2}\right)}^{\frac{2\pi}{T_M}\left(W_s+\frac{W_{cs}}{2}\right)} \frac{N_s T_M}{2W_{cs}\pi} e^{-j\left(\frac{2\pi x\nu}{T_M}\right)} dx \\ &= \frac{2N_s j}{W_{cs}\pi\nu} e^{-j\left(\frac{2W_s\pi\nu}{T_M}\right)} \sin\left(\frac{W_{cs}\pi\nu}{T_M}\right). \end{aligned} \tag{4}$$

The maximum value of $\overline{N_t}$ is achieved when W_{cs} approaches zero:

$$\begin{aligned} \text{if: } W_{cs}\to 0 \Rightarrow \left[\frac{T_M}{W_{cs}\pi\nu}\sin\left(\frac{W_{cs}\pi\nu}{T_M}\right)\right] \to 1 \\ \Rightarrow \overline{N_{t_{max}}} = \frac{2N_s}{T_M} e^{-j\left(\frac{2W_s\pi\nu}{T_M}\right)}. \end{aligned} \tag{5}$$

Therefore, the conductor distribution factor is given by:

$$\begin{aligned} K_T = \frac{T_M}{W_{cs}\pi\nu}\sin\left(\frac{W_{cs}\pi\nu}{T_M}\right) \xrightarrow{T_M=2\pi r} \\ K_T = \frac{2r}{W_{cs}\nu}\sin\left(\frac{W_{cs}\nu}{2r}\right), \end{aligned} \tag{6}$$

which can be reformulated in a more generalized form through

Table II
WINDING FACTOR FUNDAMENTAL COMPONENTS FOR VARIOUS VALUES OF K.

K	2/3	4/3	10/12	14/12	8/9	10/9
0.30	0.77	0.96	0.86	0.95	0.88	0.95
0.40	0.74	0.97	0.83	0.94	0.85	0.93
0.50	0.70	0.95	0.79	0.92	0.81	0.90
0.60	0.66	0.93	0.75	0.88	0.77	0.86
0.70	0.62	0.89	0.70	0.84	0.73	0.82
0.80	0.57	0.84	0.65	0.79	0.68	0.77
0.90	0.52	0.78	0.60	0.73	0.62	0.71
1.00	0.48	0.72	0.55	0.66	0.57	0.65

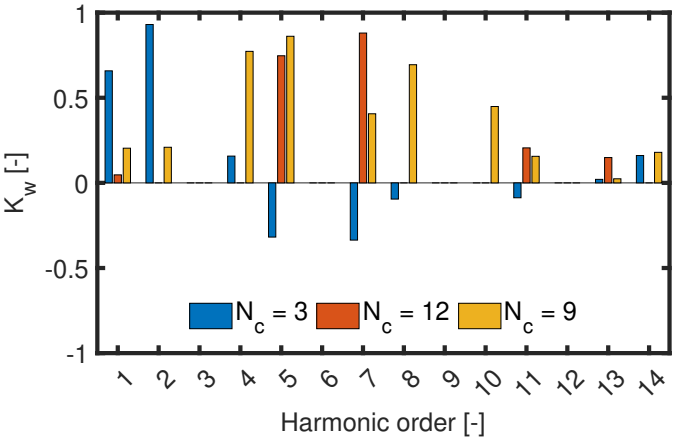

Fig. 7. Harmonic distribution of the winding factor for $K = 0.6$.

the following manipulation:

$$W_c = \frac{2\pi r}{N_c} \Rightarrow \tau_c = \frac{\pi r}{N_c} \xrightarrow{\text{if } K=\frac{W_{cs}}{\tau_c}} K_T = \frac{2N_c}{K\pi\nu}\sin\left(\frac{K\pi\nu}{2N_c}\right), \tag{7}$$

where N_c denotes the base coil number for each pole-to-coil ratio, as specified in Table I. The value of the parameter K varies with the radius at which the distribution factor is calculated. The effect of radius on coil pitch using a coreless AFPM machine with a 4/3 pole/coil combination is illustrated in Fig. 3. As the radius increases, the coil pitch expands while the coil side width remains constant, reducing the K.

Alternatively, Equation 6 can be reformulated based on the coil's inner edge radius, r_i, and the calculation radius, r. Considering the coil geometry illustrated in Fig. 6, K_T can be calculated as:

$$W_{cs} = \tau_c - \frac{W_b}{2} = \frac{\pi r}{N_c} - \frac{\pi\left(r - r_i\right)}{N_c} = \frac{\pi r_i}{N_c}$$
$$\Rightarrow K_T = \frac{2N_c r}{\pi r_i \nu}\sin\left(\frac{\pi r_i \nu}{2N_c r}\right). \tag{8}$$

B. Pitch Factor

In concentrated windings, the coils are short-pitched, leading to reduced flux linkage compared to fully pitched windings. The coil pitch factor, which quantifies the ratio of the induced voltage in short-pitched windings to that in fully pitched, is influenced by the winding configuration and the pole-to-coil ratio. Additionally, in coreless stator AFPM machines, the pitch factor is further affected by the curvature effect, where the coil side-to-pitch ratio depends on the radii.

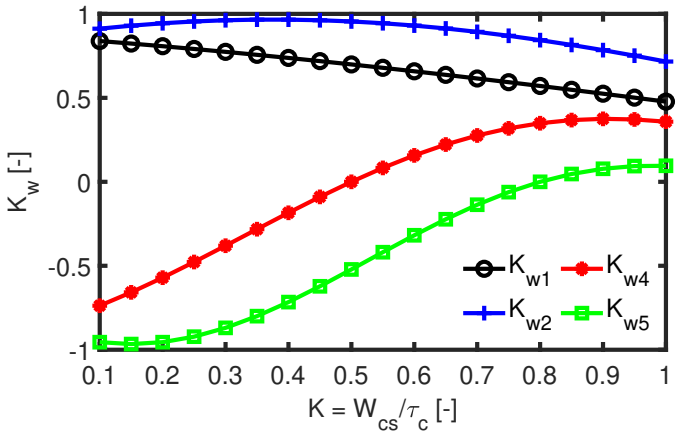

Fig. 8. Winding factor for different values of K in 4/3 configuration.

As the coils extend to larger radii, the ratio of the coil side width to the coil pitch decreases, limiting the ability to fully capture the pole flux across the entire coil pitch. The impact of chording on flux linkage is visually demonstrated in Fig. 5.

As illustrated in Fig. 4, a concentrated coil is composed of individual conductors, each spanning a pitch of $W_c - W_{cs}$. Consequently, the pitch factor for a single conductor is determined using:

$$K_p = \sin\left(\frac{\nu\pi\left(W_c - W_{cs}\right)}{T_M}\right) \xrightarrow{W_c=\frac{T_M}{N_c}} K_p =$$

$$\begin{cases} \sin\left(\dfrac{\nu\pi\left(2-K\right)}{2N_c}\right) & , \text{ for } W_{cs} = \dfrac{KW_c}{2} \\ \sin\left(\dfrac{\nu\pi\left(2r-r_i\right)}{2rN_c}\right) & , \text{ for } K = \dfrac{W_{cs}}{\tau_c} = \dfrac{r_i}{r} \end{cases} \tag{9}$$

C. Coil Group Factor

For pole-to-coil ratios of 10/12 and 14/12, two coils of the same phase are grouped, and in the 10/9 and 8/9 configurations, three coils of the same phase are grouped. Therefore, the winding factor calculations must incorporate a coil group factor. The coil group factor equals one for ratios of 2/3 and 4/3, as the coils of different phases are evenly distributed in the stator. For the 10/12 and 14/12 configurations, this factor can be determined using:

$$K_g^{N_c=12} = \frac{1}{4}\left(e^{-j0} - e^{-j\frac{\pi\nu}{6}} - e^{-j\pi\nu} + e^{-j\frac{7\pi\nu}{6}}\right). \tag{10}$$

When ν is even, K_g becomes zero, and for an odd value of ν, it is equal to:

$$K_g^{N_c=12} = \sin\left(\frac{\pi\nu}{12}\right) \tag{11}$$

Similarly, the coil group factor for the 8/9 and 10/9 configurations can be determined using the following equation:

$$K_g^{N_c=9} = \frac{1}{3}\left(e^{-j0} - e^{-j\frac{2\pi\nu}{9}} + e^{-j\frac{4\pi\nu}{9}}\right), \tag{12}$$

which is equal to:

$$K_g^{N_c=9} = \frac{1}{3}\left(2\cos\left(\frac{2\pi\nu}{9}\right) - 1\right). \tag{13}$$

IV. Comparison and Discussion

The fundamental component of the winding factor for various pole-to-coil ratios is calculated and compared in Table II, showing that the 4/3, 14/12, and 10/9 configurations exhibit higher winding factors than the others, with the 4/3 configuration achieving the highest. The harmonic distribution of the winding factor for a typical value $K = 0.6$ at average radius, for all pole-to-coil combinations, is compared in Fig. 7.

The winding factor for the 4/3 combination, which has the highest winding factor across all considered pole/coil combinations, as a function of K for multiple harmonics, is plotted in Fig. 8. It can be interpreted from the figure that as the difference between the inner and outer radii increases, the winding factor decreases at the average radius.

V. Conclusion

This paper developed generalized winding factor equations and conducted a winding harmonic analysis of coreless AFPM machines across various pole-to-coil combinations. It was demonstrated that the winding factor in these machines is a radius function, varying with different radii due to the fixed coil side width and the changing coil pitch. The conductor distribution factor, which accounts for the effect of conductor distribution in the coil sides, and the pitch factor, which captures the impact of chording in short-pitched windings, were formulated while incorporating the influence of radius. Additionally, a coil group factor was introduced and derived to account for the effect of coil grouping in pole/coil combinations with nine and twelve coils.

The winding factor for commonly used pole/coil combinations in coreless stator AFPM machines was calculated and compared across different radii and harmonic orders, assuming injecting pure sinusoid current in the windings. The results indicate that the 4/3, 10/9, and 14/12 pole/coil combinations exhibit higher winding factors and, consequently, greater torque production potential compared to other configurations, with the 4/3 configuration achieving the highest winding factor.

Acknowledgment

The support of the Leverhulme Trust, under their visiting professorship scheme, and of University of Kentucky the L. Stanley Pigman Chair in Power endowment is gratefully acknowledged. Any opinions, findings, and conclusions or recommendations expressed in this material are those of the authors and do not necessarily reflect the views of the sponsoring organizations.

References

[1] IndustryARC, "Axial flux motor market - forecast (2024 - 2030)," 2024. [Online]. Available: https://www.industryarc.com/Report/19433/axial-flux-motor-market.html

[2] F. G. Capponi, G. De Donato, and F. Caricchi, "Recent advances in axial-flux permanent-magnet machine technology," *IEEE Transactions on Industry Applications*, vol. 48, no. 6, pp. 2190–2205, 2012.

[3] F. Nishanth, J. Van Verdeghem, and E. L. Severson, "A review of axial flux permanent magnet machine technology," *IEEE Transactions on Industry Applications*, 2023.

[4] M. Aydin, S. Huang, and T. Lipo, "Axial flux permanent magnet disc machines: A review," *Conf. Record of SPEEDAM*, 01 2004.

[5] M. Vatani, Y. Chulaee, A. Mohammadi, D. R. Stewart, J. F. Eastham, and D. M. Ionel, "On the optimal design of coreless AFPM machines with Halbach array rotors for electric aircraft propulsion," in *2024 IEEE Transportation Electrification Conference and Expo (ITEC)*. IEEE, 2024, pp. 1–6.

[6] J. F. Gieras, R.-J. Wang, and M. J. Kamper, *Axial flux permanent magnet brushless machines*. Springer Science & Business Media, 2008.

[7] R. Camilleri and M. D. McCulloch, "Integrating a heat sink into concentrated wound coils to improve the current density of an axial flux, direct liquid cooled electrical machine with segmented stator," *Energies*, vol. 14, no. 12, p. 3619, 2021.

[8] F. Marcolini, G. De Donato, F. G. Capponi, and F. Caricchi, "Direct oil cooling of end-windings in torus-type axial-flux permanent-magnet machines," *IEEE Transactions on Industry Applications*, vol. 57, no. 3, pp. 2378–2386, 2021.

[9] M. Vatani, J. F. Eastham, and D. M. Ionel, "Multi-disk coreless axial flux permanent magnet synchronous motors with surface PM and Halbach array rotors for electric aircraft propulsion," in *2024 IEEE Energy Conversion Congress and Exposition (ECCE)*. IEEE, 2024, pp. 4986–4992.

[10] A. McDonald, N. Al-Khayat, D. Belshaw, M. Ravilious, A. Kumaraperumal, A. Benatamane, M. Galbraith, D. Staton, K. Benoit, and M. Mueller, "1mw multi-stage air-cored permanent magnet generator for wind turbines," in *6th IET International Conference on Power Electronics, Machines and Drives (PEMD 2012)*. IET, 2012, pp. 1–6.

[11] M. Vatani, Y. Chulaee, J. F. Eastham, and D. M. Ionel, "Analytical and fe modeling for the design of coreless axial flux machines with Halbach array and surface PM rotors," in *2024 IEEE Energy Conversion Congress and Exposition (ECCE)*. IEEE, 2024, pp. 5205–5211.

[12] N. Chayopitak and D. G. Taylor, "Performance assessment of air-core linear permanent-magnet synchronous motors," *IEEE transactions on magnetics*, vol. 44, no. 10, pp. 2310–2316, 2008.

[13] Y. Chulaee, A. Mohammadi, M. Vatani, and D. M. Ionel, "Fault-tolerant axial flux coreless PM machines with independent phase modules," in *2024 IEEE Transportation Electrification Conference and Expo (ITEC)*. IEEE, 2024, pp. 1–5.

[14] F. Y. Notash, M. Vatani, J. He, and D. M. Ionel, "Model predictive control of 5l-anpc inverter fed coreless AFPM motor with mitigated cmv in electric aircraft propulsion," in *2024 IEEE Energy Conversion Congress and Exposition (ECCE)*. IEEE, 2024, pp. 2498–2505.

[15] M. Vatani, Y. Chulaee, J. F. Eastham, X. Pei, and D. M. Ionel, "Multi-wound axial flux generators with Halbach array rotors," in *2024 IEEE Energy Conversion Congress and Exposition (ECCE)*. IEEE, 2024, pp. 5199–5204.

[16] F. Marignetti, G. Volpe, S. M. Mirimani, and C. Cecati, "Electromagnetic design and modeling of a two-phase axial-flux printed circuit board motor," *IEEE Transactions on Industrial Electronics*, vol. 65, no. 1, pp. 67–76, 2017.

[17] F. Marcolini, G. De Donato, F. G. Capponi, and F. Caricchi, "Design of a high speed printed circuit board coreless axial flux permanent magnet machine," in *2021 IEEE Energy Conversion Congress and Exposition (ECCE)*. IEEE, 2021, pp. 4353–4360.

[18] Y. Chulaee, D. Lewis, M. Vatani, J. F. Eastham, and D. M. Ionel, "Torque and power capabilities of coreless axial flux machines with surface PMs and Halbach array rotors," in *2023 IEEE International Electric Machines & Drives Conference (IEMDC)*. IEEE, 2023, pp. 1–6.

[19] S. Neethu, S. P. Nikam, S. Singh, S. Pal, A. K. Wankhede, and B. Fernandes, "High-speed coreless axial-flux permanent-magnet motor with printed circuit board winding," *IEEE Transactions on Industry Applications*, vol. 55, no. 2, pp. 1954–1962, 2018.

[20] Infinitum Electric, "Infinitum Electric - High-Efficiency Electric Machines," 2025. [Online]. Available: https://goinfinitum.com/

[21] PCB Stator Technology, "PCB Stator Technology - High-Efficiency Electric Motors," 2025. [Online]. Available: https://pcbstator.com/

[22] S. Butterfield, J. Smith, D. Petch, B. Sullivan, P. Smith, and K. Pierce, "Advanced gearless drivetrain-phase I technical report," Boulder Wind Power, Inc., Tech. Rep., 2012.

[23] W. Yan, X. Pei, H. Wang, Y. Wang, J. F. Eastham, and X. Zeng, "Topology optimization of a fully superconducting air-core motor for electric aircraft," *IEEE Transactions on Applied Superconductivity*, 2025.

[24] LaunchPoint EPS, "Motors & generators," 2025. [Online]. Available: https://launchpointeps.com/motors-generators/

[25] M. R. Ricci, J. G. Sugar, B. E. Paden, and D. B. Paden, "Axial flux brushless permanent magnet electrical machine rotor," Nov. 27 2018, US Patent 10,141,822.

[26] G. A. Long, B. E. Paden, M. R. Ricci, D. B. Paden, and J. G. Sugar, "Lightweight and efficient electrical machine and method of manufacture," Feb. 25 2020, US Patent 10,574,110.

[27] M. A. Mueller and A. S. McDonald, "A lightweight low-speed permanent magnet electrical generator for direct-drive wind turbines," *Wind Energy: An International Journal for Progress and Applications in Wind Power Conversion Technology*, vol. 12, no. 8, pp. 768–780, 2009.

[28] I. Subotic, C. Gammeter, A. Tüysüz, and J. W. Kolar, "Weight optimization of an axial-flux PM machine for airborne wind turbines," in *2016 IEEE International Conference on Power Electronics, Drives and Energy Systems (PEDES)*. IEEE, 2016, pp. 1–6.

[29] H. Cimen and M. Mueller, "6-rpm 5MW axial flux multi-stage air cored permanent magnet generator design for vertical axis offshore wind turbines," in *11th International Conference on Power Electronics, Machines and Drives (PEMD 2022)*, vol. 2022. IET, 2022, pp. 395–399.

[30] M. Chirca, S. Breban, C. Oprea, and M. M. Radulescu, "Comparative design analysis of ferrite-permanent-magnet micro-wind turbine generators," in *2015 Intl Aegean Conference on Electrical Machines & Power Electronics (ACEMP)*. IEEE, 2015, pp. 687–692.

[31] M. A. Mueller, J. Burchell, Y. C. Chong, O. Keysan, A. McDonald, M. Galbraith, and E. J. E. Subiabre, "Improving the thermal performance of rotary and linear air-cored permanent magnet machines for direct drive wind and wave energy applications," *IEEE Transactions on Energy Conversion*, vol. 34, no. 2, pp. 773–781, 2018.

[32] S. P. Colyer, P. Arumugam, and J. F. Eastham, "Modular airgap windings for linear permanent magnet machines," *IET Electric Power Applications*, vol. 12, no. 7, pp. 953–961, 2018.

[33] S. G. Min and B. Sarlioglu, "3-d performance analysis and multiobjective optimization of coreless-type PM linear synchronous motors," *IEEE Transactions on Industrial Electronics*, vol. 65, no. 2, pp. 1855–1864, 2017.

[34] ——, "Analytical calculation of back EMF waveform for linear PM motors in slotted and slotless structures," *IEEE Transactions on Magnetics*, vol. 53, no. 12, pp. 1–10, 2017.

[35] F. Libert and J. Soulard, "Investigation on pole-slot combinations for permanent-magnet machines with concentrated windings," in *Proc. ICEM*, 2004, pp. 530–535.